

# Fully Conjugated Phthalocyanine Copper Metal–Organic Frameworks for Sodium–Iodine Batteries with Long-Time-Cycling Durability

Faxing Wang, Zaichun Liu, Chongqing Yang, Haixia Zhong, Gyutae Nam, Panpan Zhang, Renhao Dong, Yuping Wu, Jaephil Cho, Jian Zhang,\* and Xinliang Feng\*

Rechargeable sodium–iodine (Na–I<sub>2</sub>) batteries are attracting growing attention for grid-scale energy storage due to their abundant resources, low cost, environmental friendliness, high theoretical capacity (211 mAh g<sup>-1</sup>), and excellent electrochemical reversibility. Nevertheless, the practical application of Na–I<sub>2</sub> batteries is severely hindered by their poor cycle stability owing to the serious dissolution of polyiodide in the electrolyte during charge/discharge processes. Herein, the atomic modulation of metal–bis(dihydroxy) species in a fully conjugated phthalocyanine copper metal–organic framework (MOF) for suppression of polyiodide dissolution toward long-time cycling Na–I<sub>2</sub> batteries is demonstrated. The Fe<sub>2</sub>[(2,3,9,10,16,17,23,24-octahydroxy phthalocyaninato)Cu] MOF composited with I<sub>2</sub> (Fe<sub>2</sub>–O<sub>8</sub>–PcCu/I<sub>2</sub>) serves as a cathode for a Na–I<sub>2</sub> battery exhibiting a stable specific capacity of 150 mAh g<sup>-1</sup> after 3200 cycles and outperforming the state-of-the-art cathodes for Na–I<sub>2</sub> batteries. Operando spectroelectrochemical and electrochemical kinetics analyses together with density functional theory calculations reveal that the square planar iron–bis(dihydroxy) (Fe–O<sub>4</sub>) species in Fe<sub>2</sub>–O<sub>8</sub>–PcCu are responsible for the binding of polyiodide to restrain its dissolution into electrolyte. Besides the monovalent Na–I<sub>2</sub> batteries in organic electrolytes, the Fe<sub>2</sub>–O<sub>8</sub>–PcCu/I<sub>2</sub> cathode also operates stably in other metal–I<sub>2</sub> batteries like aqueous multivalent Zn–I<sub>2</sub> batteries. Thus, this work offers a new strategy for designing stable cathode materials toward high-performance metal–iodine batteries.


Currently, lithium-ion batteries (LIBs) are the most widely used electrochemical energy storage devices for portable electronics. However, the rarity and unreasonably high cost of lithium resources hinders the extensive utilizations of LIBs for storing the electricity generated from intermittent renewable energy. Thus, it is crucial to develop new battery technologies based on earth-abundant elements. Rechargeable sodium–iodine (Na–I<sub>2</sub>) batteries are such appealing alternative power sources to the prevailing LIBs because of the natural abundance and low price of both sodium and iodine (high reserves in the ocean: 10 g<sub>sodium</sub> L<sub>ocean</sub><sup>-1</sup> and 55 μg<sub>iodine</sub> L<sub>ocean</sub><sup>-1</sup>), environmentally friendly characteristic, high theoretical capacity (211 mAh g<sup>-1</sup>), etc.<sup>[4–15]</sup> For Na–I<sub>2</sub> batteries in organic electrolytes, the electrochemical reactions of I<sub>2</sub> cathodes principally occur as following: I<sub>2</sub> ↔ NaI<sub>3</sub> ↔ NaI.<sup>[6–8]</sup> However, the dissolution and diffusion of polyiodide intermediate (NaI<sub>3</sub>) into the electrolyte cause serious capacity deterioration and low columbic efficiency of Na–I<sub>2</sub> batteries.<sup>[6–8]</sup> Meanwhile, sluggish redox kinetics of polyiodide results in extremely poor rate capability of Na–I<sub>2</sub> batteries.<sup>[6–8]</sup> To address above issues, various carbonaceous materials (graphene, carbon cloths, hollow carbon, heteroatom-doped carbon, etc.)

The development of grid-scale electrochemical storage systems for intermittent renewable energy sources urgently requires the exploration of cost-effective and sustainable battery systems.<sup>[1–3]</sup>

results in extremely poor rate capability of Na–I<sub>2</sub> batteries.<sup>[6–8]</sup> To address above issues, various carbonaceous materials (graphene, carbon cloths, hollow carbon, heteroatom-doped carbon, etc.)

F. Wang, Dr. H. Zhong, P. Zhang, Dr. R. Dong, Prof. J. Zhang, Prof. X. Feng  
Center for Advancing Electronics Dresden (cfaed) and Department  
of Chemistry and Food Chemistry  
Technische Universität Dresden  
01062 Dresden, Germany  
E-mail: xinliang.feng@tu-dresden.de

Z. Liu, Prof. Y. Wu  
School of Energy Science and Engineering  
and Institute for Advanced Materials  
Nanjing Tech University  
Nanjing 211816, Jiangsu Province, China

 The ORCID identification number(s) for the author(s) of this article can be found under <https://doi.org/10.1002/adma.201905361>.

© 2019 The Authors. Published by WILEY-VCH Verlag GmbH & Co. KGaA, Weinheim. This is an open access article under the terms of the Creative Commons Attribution License, which permits use, distribution and reproduction in any medium, provided the original work is properly cited.

DOI: 10.1002/adma.201905361

Dr. C. Yang, Prof. X. Feng  
School of Chemistry and Chemical Engineering  
Shanghai Jiao Tong University  
Shanghai 200240, China

Dr. G. Nam, Prof. J. Cho  
School of Energy and Chemical Engineering  
Ulsan National Institute of Science and Technology (UNIST)  
Ulsan 44919, South Korea

Prof. J. Zhang  
Department of Applied Chemistry  
School of Applied and Natural Sciences  
Northwestern Polytechnical University  
Xi'an 710129, China  
E-mail: zhangjian@nwpu.edu.cn

with porous structures have been utilized to encapsulate  $I_2$  as cathodes.<sup>[4–8,12]</sup> Typically, carbon materials can serve as physical barriers to suppress the polyiodide dissolution and buffer the volume expansion/contraction of active  $I_2$  electrodes for metal– $I_2$  batteries.<sup>[4–8,12]</sup> Unfortunately, owing to the poor affinity between the nonpolar carbons and polar polyiodides, the polyiodide dissolution and diffusion cannot be thoroughly eliminated. Another common material for immobilizing polyiodide is the poly(vinylpyrrolidone) (PVP), which can form hydrogen bonds with polyiodides.<sup>[14]</sup> However, the extremely poor electrical conductivity of PVP brings about sluggish electrochemical redox kinetics and poor rate capability of metal– $I_2$  batteries. Consequently, it is particularly desirable to explore efficient electrode materials for high-performance metal– $I_2$  batteries.

Benefitting from their atomically dispersed metal centers, abundant pore structures and superior electrical conductivities, layered conjugated metal–organic frameworks (MOFs) with weak and out-plane  $\pi$ – $\pi$  stacking are theoretically attractive for addressing present bottlenecks of the  $I_2$  cathode. First, dense metal centers in MOFs have stronger polarity than carbon atoms, which will yield strong chemisorption capability toward iodide and polyiodide.<sup>[16–18]</sup> Second, the extended  $\pi$ -conjugation within the conjugated MOFs has greatly improved electron transfer ability compared with traditionally non-conductive MOFs and PVP,<sup>[19–21]</sup> which will promote the redox kinetics of polyiodide. Third, porous nanostructure of the conjugated MOFs is beneficial for a large amount of  $I_2$  loading, simultaneously alleviating the volume changes and contributing to fast electrolyte penetration. Significantly, the modulation of metal–ligand orbital hybridization in the conjugated MOFs allows for profound investigations on the charge storage mechanisms at the molecular level.<sup>[22–29]</sup> Nevertheless, conjugated MOFs still remain unexplored for metal– $I_2$  batteries.

In this work, we demonstrated fully conjugated polyphthalocyanine copper metal–organic frameworks (PcCu-MOFs) with atomically tunable metal–ligand orbital hybridization for suppressing polyiodide dissolution to enhance the cycle stability of Na– $I_2$  batteries. Operando spectroelectrochemical measurements, electrochemical kinetics analyses, together with density functional theory (DFT) calculations reveal that intrinsic metal-bis(dihydroxy) species of  $Fe_2[(2,3,9,10,16,17,23,24\text{-octahydroxy phthalocyaninato})Cu]$  ( $Fe_2-O_8-PcCu$ ) have strong polarization toward the polyiodide, thus effectively preventing the polyiodide dissolution into the electrolyte. As a result, the  $Fe_2-O_8-PcCu/I_2$  manifests a high specific capacity of 208 mAh g<sup>-1</sup> and excellent rate capability up to 2.5 A g<sup>-1</sup>. Remarkably, the Na– $I_2$  battery using the  $Fe_2-O_8-PcCu/I_2$  as a cathode performs a long-term cycle stability up to 3200 cycles, outperforming currently reported Na– $I_2$  batteries (<2000 cycles).

Three fully conjugated PcCu-MOFs (Figure 1a) with 2,3,9,10,16,17,23,24-octahydroxy phthalocyaninato coppers as building blocks and metal–bis(dihydroxy) complexes as linkages were synthesized using a solvothermal protocol.<sup>[27,30]</sup> As shown in scanning electron microscopy (SEM) images, the sizes of as-synthesized  $Fe_2-O_8-PcCu$ ,  $Ni_2-O_8-PcCu$  ( $Ni_2[(2,3,9,10,16,17,23,24\text{-octahydroxy phthalocyaninato})Cu]$ ) and  $Zn_2-O_8-PcCu$  ( $Zn_2[(2,3,9,10,16,17,23,24\text{-octahydroxy phthalocyaninato})Cu]$ ) ranged from 0.3 to 1  $\mu$ m (Figure S1, Supporting Information). Using a melt diffusion method at 115 °C

(Figure S2, Supporting Information),  $I_2$  molecules with various weight fractions (10–45%) were loaded into the  $Fe_2-O_8-PcCu$ ,  $Ni_2-O_8-PcCu$ , and  $Zn_2-O_8-PcCu$ . The corresponding elemental mapping images (Figure 1b; Figure S3, Supporting Information), thermogravimetric analysis (Figure S4a, Supporting Information), and nitrogen adsorption–desorption tests (Figure S4b, Supporting Information) confirmed the homogeneous dispersion of elemental iodine in PcCu-MOFs. Moreover, the experimentally achieved powder X-ray diffraction (XRD) patterns matched well with the computationally simulated XRD patterns of  $Fe_2-O_8-PcCu$  with AA-stacking configurations (Figure 1c), unambiguously indicating their stable crystalline structures with long-range orders at the (100)/(010) plane and layer stacking structures along the [001] direction. In addition, the XRD peaks at  $\approx 25^\circ$  in all three samples were indexed to the (109) crystal planes of  $I_2$ . The measured electrical conductivities of the pressed  $Fe_2-O_8-PcCu/I_2$ ,  $Ni_2-O_8-PcCu/I_2$ , and  $Zn_2-O_8-PcCu/I_2$  pellets with the same loading amount of  $I_2$  reached  $\approx 9.7$ , 8.3, and 6.9 mS cm<sup>-1</sup> at room temperature, respectively (Figure S5, Supporting Information). Considering the highest electrical conductivity of  $Fe_2-O_8-PcCu/I_2$  among above three composites, X-ray absorption fine structure (XAFS) measurements were performed to investigate the structural variation of  $Fe_2-O_8-PcCu$  and  $Fe_2-O_8-PcCu/I_2$  composites (Figure S6a, Supporting Information). The related Fourier transform (FT) curve of extended X-ray absorption fine structure (EXAFS) of  $Fe_2-O_8-PcCu/I_2$  presents the Fe–O coordination peak at about  $\approx 1.56$  Å and no Fe–Fe path at  $\approx 2.9$  Å (Figure S6b, Supporting Information).<sup>[30,31]</sup> The X-ray photoelectron spectroscopy (XPS) analysis of  $Fe_2-O_8-PcCu$  and  $Fe_2-O_8-PcCu/I_2$  reveals the presence of C, N, O, Fe, and Cu elements in the  $Fe_2-O_8-PcCu$  and the presence of I, C, N, O, Fe, and Cu elements in  $Fe_2-O_8-PcCu/I_2$  (Figures S6c–l, Supporting Information). The deconvoluted O 1s XPS spectrum (Figure 1d; Figure S6e, Supporting Information) can be fitted into Fe–O peak (533.5 eV) and C–O peak (531.9 eV) due to the coordination of C–O and the Fe atoms.<sup>[30]</sup> The N 1s XPS spectrum consists of two peaks of Cu–N at 398.5 eV and N–H at 401 eV (Figure 1e; Figure S6f, Supporting Information), suggesting the coordination of N atoms and Cu ions.<sup>[30]</sup> Notably, the binding energy of I 2p<sub>5/2</sub> peak at 620.1 eV (Figure 1f) is higher than that in  $CuI_2$  (619 eV),<sup>[32]</sup> indicating the free iodine in the  $Fe_2-O_8-PcCu/I_2$  composite without Cu–I bonds. Generally, no Fe–I and Cu–I bonds were observed in EXAFS and XPS analyses, suggesting the physical adsorption of  $I_2$  in  $Fe_2-O_8-PcCu$ .

The electrochemical performance of  $Fe_2-O_8-PcCu/I_2$ ,  $Ni_2-O_8-PcCu/I_2$  and  $Zn_2-O_8-PcCu/I_2$  composites as cathodes for Na– $I_2$  batteries (Figure S7a, Supporting Information) were evaluated using cyclic voltammogram (CV) and galvanostatic charge/discharge measurements. First, CV curves at various scan rates were collected to evaluate the electrochemical contributions of PcCu-MOF/ $I_2$  electrodes (Figure S7b–d, Supporting Information). The total current at each voltage in CV curves can be divided into a diffusion-controlled current and a surface-controlled (or capacitive) current according to the equation of  $i = k_1\nu + k_2\nu^{1/2}$ , where the  $i$ ,  $\nu$ ,  $k_1\nu$ , and  $k_2\nu^{1/2}$  represent the total current, scan rate, capacitive-dominated current, and diffusion-controlled current, respectively.<sup>[33–35]</sup> For the

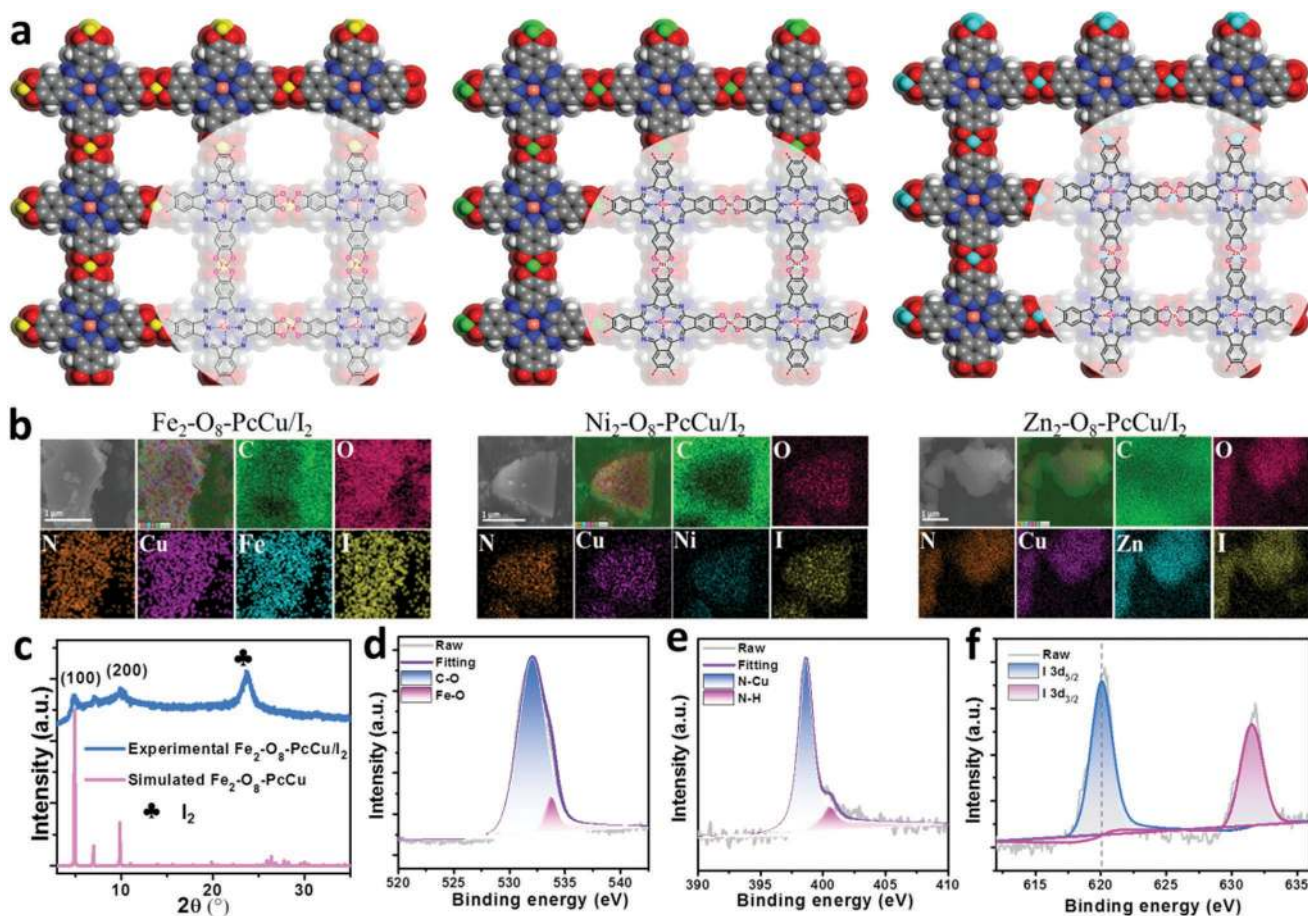


**Figure 1.** a) Schematic modeling and chemical structures of layered conjugated PcCu-MOFs (gray: carbon; red: oxygen; white: hydrogen; blue: nitrogen; pink: cuprum; yellow: iron; green: nickel; sky blue: zinc). b) SEM images and corresponding elemental mapping images of Fe<sub>2</sub>-O<sub>8</sub>-PcCu/I<sub>2</sub>, Ni<sub>2</sub>-O<sub>8</sub>-PcCu/I<sub>2</sub>, and Zn<sub>2</sub>-O<sub>8</sub>-PcCu/I<sub>2</sub> composites. c) The experimental powder XRD patterns of Fe<sub>2</sub>-O<sub>8</sub>-PcCu/I<sub>2</sub> with the simulated XRD patterns of Fe<sub>2</sub>-O<sub>8</sub>-PcCu. d–f) The O 2p, N 1s, and I 3d XPS spectra of Fe<sub>2</sub>-O<sub>8</sub>-PcCu/I<sub>2</sub>.

Fe<sub>2</sub>-O<sub>8</sub>-PcCu/I<sub>2</sub> electrode, the identified capacitive contribution was  $\approx 41\%$  of the total capacity at  $2 \text{ mV s}^{-1}$  (Figure 2a). When the scan rate increased to  $8 \text{ mV s}^{-1}$ , the capacitive contribution ratio reached to 58% (Figure 2b). Generally, the I<sub>2</sub>/NaI redox reactions are dominated by the diffusion-controlled charge storage processes.<sup>[6–8]</sup> Thus, the capacitive contribution in the Fe<sub>2</sub>-O<sub>8</sub>-PcCu/I<sub>2</sub> electrode is associated with the intrinsic capacitive behavior of the conjugated PcCu-MOFs.<sup>[20,21]</sup> Because of the existence of both capacitive and diffusion-controlled charge storage, a high I<sub>2</sub> loading in PcCu-MOF/I<sub>2</sub> composites cannot lead to an increased specific capacity (Figure S8a, Supporting Information). The optimal weight fraction of I<sub>2</sub> in PcCu-MOF/I<sub>2</sub> was  $\approx 40\%$  (Figure S8, Supporting Information).

Subsequently, the cycling behaviors of Fe<sub>2</sub>-O<sub>8</sub>-PcCu/I<sub>2</sub>, Ni<sub>2</sub>-O<sub>8</sub>-PcCu/I<sub>2</sub>, and Zn<sub>2</sub>-O<sub>8</sub>-PcCu/I<sub>2</sub> electrodes with the same loading content of I<sub>2</sub> (40%, wt%) were evaluated at  $0.3 \text{ A g}^{-1}$ . After 100 cycles, capacity retention of Fe<sub>2</sub>-O<sub>8</sub>-PcCu/I<sub>2</sub> was remarkably up to 100% ( $208 \text{ mAh g}^{-1}$ ), which was substantially higher than 65% ( $132 \text{ mAh g}^{-1}$ ) for Ni<sub>2</sub>-O<sub>8</sub>-PcCu/I<sub>2</sub> and 33% ( $67 \text{ mAh g}^{-1}$ ) for Zn<sub>2</sub>-O<sub>8</sub>-PcCu/I<sub>2</sub> (Figure 2c). The capacity deterioration for the Ni<sub>2</sub>-O<sub>8</sub>-PcCu/I<sub>2</sub> and Zn<sub>2</sub>-O<sub>8</sub>-PcCu/I<sub>2</sub> electrodes was derived from the dissolution of polyiodide instead of the structural instability of Ni<sub>2</sub>-O<sub>8</sub>-PcCu and

Zn<sub>2</sub>-O<sub>8</sub>-PcCu (Figure S9, Supporting Information). Notably, at a relatively low current density of  $0.3 \text{ A g}^{-1}$ , all these PcCu-MOF/I<sub>2</sub> electrodes exhibited high specific capacities in the range of  $204\text{--}208 \text{ mAh g}^{-1}$ . However, when the current density reached  $1.5 \text{ A g}^{-1}$ , the Fe<sub>2</sub>-O<sub>8</sub>-PcCu/I<sub>2</sub> electrode delivered a higher discharge capacity of  $157 \text{ mAh g}^{-1}$  (Figure 2d) than Ni<sub>2</sub>-O<sub>8</sub>-PcCu/I<sub>2</sub> ( $118 \text{ mAh g}^{-1}$ ) and Zn<sub>2</sub>-O<sub>8</sub>-PcCu/I<sub>2</sub> ( $110 \text{ mAh g}^{-1}$ ) electrodes (Figure S10, Supporting Information). Even at a higher current density of  $2.5 \text{ A g}^{-1}$ , the Fe<sub>2</sub>-O<sub>8</sub>-PcCu/I<sub>2</sub> electrode still retained a discharge capacity of  $127 \text{ mAh g}^{-1}$ , corresponding to 61% capacity retention of the initial discharge capacity at  $0.3 \text{ A g}^{-1}$ . Generally, the Fe<sub>2</sub>-O<sub>8</sub>-PcCu/I<sub>2</sub> electrode displayed better cycle stability and superior rate capability than Ni<sub>2</sub>-O<sub>8</sub>-PcCu/I<sub>2</sub> and Zn<sub>2</sub>-O<sub>8</sub>-PcCu/I<sub>2</sub> electrodes (Figure S11, Supporting Information). Markedly, after 3200 cycles at  $1.5 \text{ A g}^{-1}$ , the specific capacity of Fe<sub>2</sub>-O<sub>8</sub>-PcCu/I<sub>2</sub> electrode was as high as of  $150 \text{ mAh g}^{-1}$  (Figure 2e), demonstrating the superior cycling stability among almost all of the reported I<sub>2</sub>-based electrodes for metal-I<sub>2</sub> batteries (Table S1, Supporting Information), e.g., Li-I<sub>2</sub> batteries ( $<4000$  cycles),<sup>[12,36–41]</sup> Na-I<sub>2</sub> batteries ( $<2000$  cycles),<sup>[4–7]</sup> Mg-I<sub>2</sub> batteries ( $<200$  cycles),<sup>[8,42]</sup> Zn-I<sub>2</sub> batteries ( $<3000$  cycles),<sup>[15,43,44]</sup> Al-I<sub>2</sub> batteries ( $<1000$  cycles)<sup>[14]</sup> and metal-I<sub>2</sub> flow batteries ( $<500$  cycles).<sup>[9–11,45,46]</sup> As shown in Figure S12a



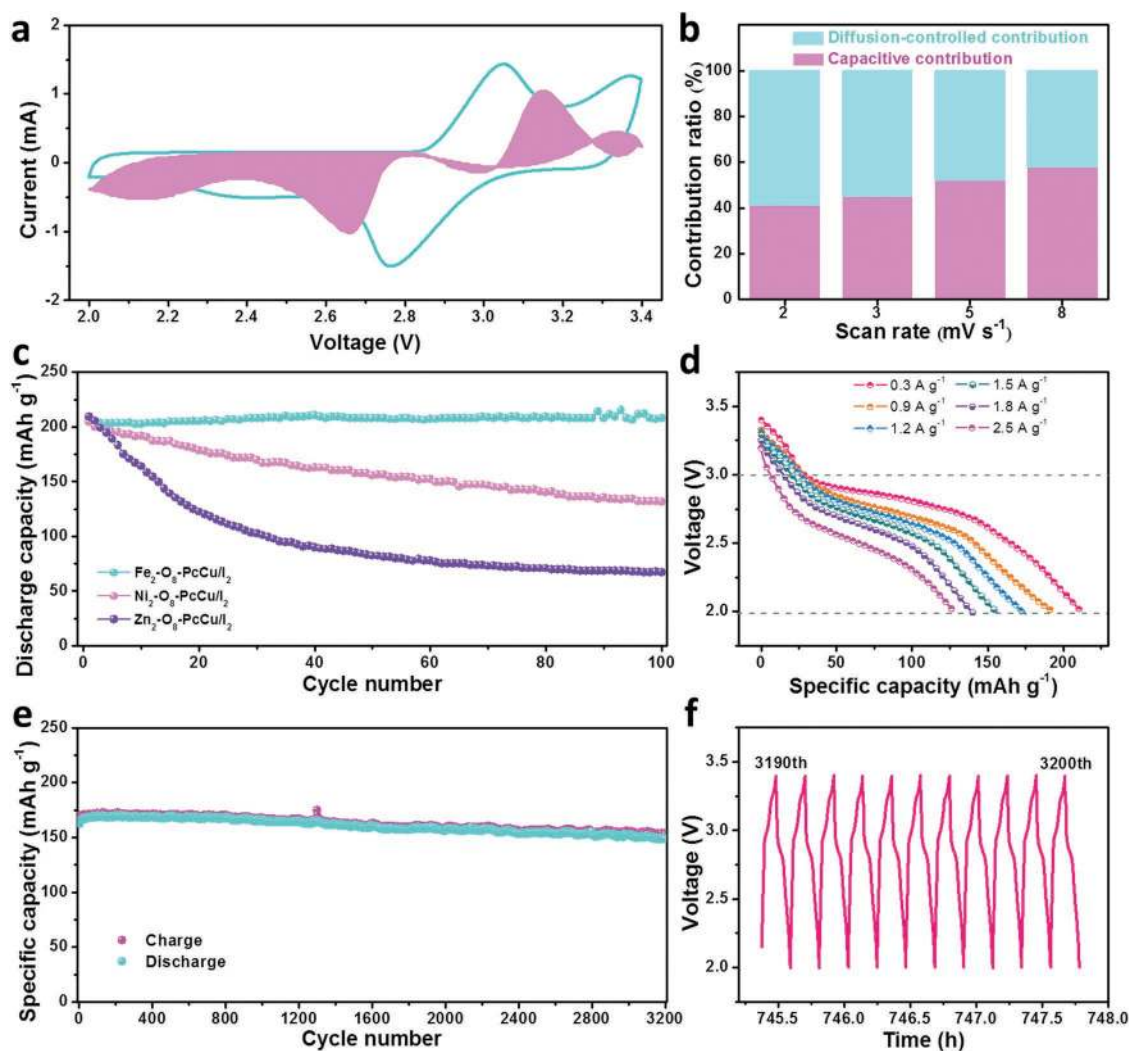


**Figure 2.** The electrochemical properties of the PcCu-MOF/I<sub>2</sub> composites for Na-I<sub>2</sub> batteries. a) CV curve of Fe<sub>2</sub>-O<sub>8</sub>-PcCu/I<sub>2</sub> electrode at 2 mV s<sup>-1</sup>. The capacitive contribution is shown in the shaded area. b) Relative contribution ratios of the capacitive and diffusion-controlled charge storage in the Fe<sub>2</sub>-O<sub>8</sub>-PcCu/I<sub>2</sub> electrode at various scan rates. c) The cycle behaviors of the Fe<sub>2</sub>-O<sub>8</sub>-PcCu/I<sub>2</sub>, Ni<sub>2</sub>-O<sub>8</sub>-PcCu/I<sub>2</sub>, and Zn<sub>2</sub>-O<sub>8</sub>-PcCu/I<sub>2</sub> electrodes at 0.3 A g<sup>-1</sup>. d) The galvanostatic discharge profiles of the Fe<sub>2</sub>-O<sub>8</sub>-PcCu/I<sub>2</sub> electrodes at various current densities. e) The long-time cycle of the Fe<sub>2</sub>-O<sub>8</sub>-PcCu/I<sub>2</sub> electrodes at 1.5 A g<sup>-1</sup> and f) corresponding voltage-time curves.

(Supporting Information), after 3200 cycles at  $1.5 \text{ A g}^{-1}$ , the surface of  $\text{Fe}_2\text{-O}_8\text{-PcCu/I}_2$  electrode showed no clear fracture and the I<sub>2</sub> was still homogeneously distributed within the  $\text{Fe}_2\text{-O}_8\text{-PcCu}$ , proving the integrity of the whole electrode. Furthermore, the discharge voltages showed no fading within the whole cycle processes (Figure 2f), indicating the outstanding structural stability of the  $\text{Fe}_2\text{-O}_8\text{-PcCu/I}_2$  electrode. After the prolonged cycling tests, the Coulombic efficiency of the  $\text{Fe}_2\text{-O}_8\text{-PcCu/I}_2$  electrode was  $\approx 99.3\%$  (Figure S12b, Supporting Information), suggesting highly reversible redox reactions. Additionally, 30 commercial red light-emitting diodes were stably powered for over 20 min using the charged Na-I<sub>2</sub> battery based on  $\text{Fe}_2\text{-O}_8\text{-PcCu/I}_2$  (Figure S13, Supporting Information).

To deeply understand the structure-performance relationship of PcCu-MOF/I<sub>2</sub>, operando spectroelectrochemical measurements were conducted for Na-I<sub>2</sub> batteries based

on  $\text{Fe}_2\text{-O}_8\text{-PcCu/I}_2$ ,  $\text{Ni}_2\text{-O}_8\text{-PcCu/I}_2$ , and  $\text{Zn}_2\text{-O}_8\text{-PcCu/I}_2$  electrodes. First, the dissolution behavior of the polyiodide in the electrolyte was studied using an operando electrochemical ultraviolet-visible (UV-vis) spectroscopy (Figure S14a, Supporting Information). The strong absorption peak at the range of 290–294 nm is associated with I<sub>3</sub><sup>-</sup> in the electrolyte (Figure S15, Supporting Information).<sup>[47]</sup> The other three absorption peaks at the range of 500–800 nm result from the used organic electrolyte (Figure S14, Supporting Information). During the discharge process of the  $\text{Ni}_2\text{-O}_8\text{-PcCu/I}_2$  electrode, a I<sub>3</sub><sup>-</sup> absorption peak at 294 nm appeared (Figure 3a). Compared with  $\text{Ni}_2\text{-O}_8\text{-PcCu/I}_2$  electrode, a much stronger I<sub>3</sub><sup>-</sup> absorption peak was observed for the  $\text{Zn}_2\text{-O}_8\text{-PcCu/I}_2$  electrode after the discharge process (Figure S16, Supporting Information). Principally, the detected I<sub>3</sub><sup>-</sup> is the intermediate product during the phase transformation from I<sub>2</sub> to NaI (Figure S17, Supporting Information). The easy dissolution of I<sub>3</sub><sup>-</sup> into the electrolyte

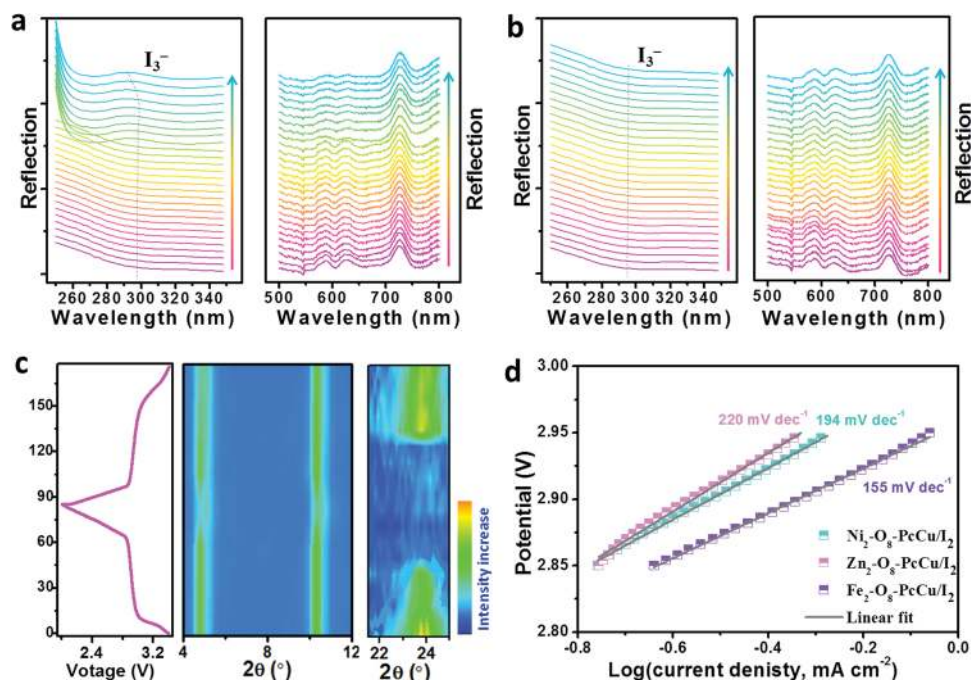


**Figure 3.** Operando spectroelectrochemical measurements and kinetic analyses of Na-I<sub>2</sub> batteries using the PcCu-MOF/I<sub>2</sub> composites. a, b) The operando electrochemical UV-vis spectroscopies of Na-I<sub>2</sub> batteries based on Ni<sub>2</sub>-O<sub>8</sub>-PcCu/I<sub>2</sub> (a) and Fe<sub>2</sub>-O<sub>8</sub>-PcCu/I<sub>2</sub> (b) electrodes during the discharge process. The arrow indicates the discharge process with the initial state at the bottom and the completed discharge state at the top. c) The operando XRD characterization of the Fe<sub>2</sub>-O<sub>8</sub>-PcCu/I<sub>2</sub> electrodes during the charge/discharge processes. d) The plots of NaI<sub>3</sub> oxidation slopes derived from potentiostatic polarization experiments on the Fe<sub>2</sub>-O<sub>8</sub>-PcCu/I<sub>2</sub>, Ni<sub>2</sub>-O<sub>8</sub>-PcCu/I<sub>2</sub>, and Zn<sub>2</sub>-O<sub>8</sub>-PcCu/I<sub>2</sub> electrodes.

leads to the loss of active material from the Ni<sub>2</sub>-O<sub>8</sub>-PcCu/I<sub>2</sub> and the Zn<sub>2</sub>-O<sub>8</sub>-PcCu/I<sub>2</sub> electrodes, which deteriorate their cycle lifespan. By contrast, the polyiodide dissolution behavior was not observed in the Fe<sub>2</sub>-O<sub>8</sub>-PcCu/I<sub>2</sub> electrode during the discharge process (Figure 3b), suggesting that the Fe-O<sub>4</sub> species in the Fe<sub>2</sub>-O<sub>8</sub>-PcCu can suppress the polyiodide dissolution better than Ni-O<sub>4</sub> species in Ni<sub>2</sub>-O<sub>8</sub>-PcCu and Zn-O<sub>4</sub> species in Zn<sub>2</sub>-O<sub>8</sub>-PcCu. Therefore, the Fe<sub>2</sub>-O<sub>8</sub>-PcCu/I<sub>2</sub> electrode presented much better cycling stability than Ni<sub>2</sub>-O<sub>8</sub>-PcCu/I<sub>2</sub> and Zn<sub>2</sub>-O<sub>8</sub>-PcCu/I<sub>2</sub> electrodes.

In order to further track the structural variation of Fe<sub>2</sub>-O<sub>8</sub>-PcCu/I<sub>2</sub> electrode during the charge/discharge processes, operando X-ray diffraction (XRD) characterization was carried out (Figure S18, Supporting Information). For the Fe<sub>2</sub>-O<sub>8</sub>-PcCu/I<sub>2</sub> electrode, the characteristic (109) peak of I<sub>2</sub> at 25° gradually disappeared during the discharge process (Figure 3c) which was due to its progressive dissociation reaction with Na ion. After 2 h, the (109) peak appeared again in the subsequent charge process, indicating reversible redox pathways. The complete restoration of the crystalline I<sub>2</sub> structure in Fe<sub>2</sub>-O<sub>8</sub>-PcCu was in good agreement with the high electrochemical reversibility in above electrochemical tests (Figure 2e,f, Supporting Information). Moreover, during the discharge process, both the (100) and (200) peaks of Fe<sub>2</sub>-O<sub>8</sub>-PcCu have slightly shifted to the high 2θ direction after 65 min (Figure 3c), meaning the layer spacing of Fe<sub>2</sub>-O<sub>8</sub>-PcCu is slightly reduced. This variation during the discharge process could be due to the formation of the triiodide-Fe<sub>2</sub>-O<sub>8</sub>-PcCu intermediate or the iodide-Fe<sub>2</sub>-O<sub>8</sub>-PcCu intermediates or the Na-Fe<sub>2</sub>-O<sub>8</sub>-PcCu intermediates from the capacitive-type charge storage. The operando X-ray

adsorption near edge structure spectra at Fe K-edge and operando synchrotron radiation X-ray photoelectron spectroscopy are promising to check the specific complexation (like valence states and bonding structures) in the future.<sup>[48,49]</sup> Notably, the (100) and (200) peaks of the Fe<sub>2</sub>-O<sub>8</sub>-PcCu were maintained after the discharge and charge processes for the redox reactions. This indicates that the interaction between the Fe<sub>2</sub>-O<sub>8</sub>-PcCu and (poly) iodide or the capacitive-type Na-ion storage in Fe<sub>2</sub>-O<sub>8</sub>-PcCu would not undermine the layer structures of PcCu-MOFs. In addition, the charge-transfer kinetics of soluble NaI<sub>3</sub> oxidation conversion on PcCu-MOFs electrodes were investigated through potentiostatic polarization experiments (Figure S19, Supporting Information). The obtained NaI<sub>3</sub> oxidation slope for Fe<sub>2</sub>-O<sub>8</sub>-PcCu/I<sub>2</sub> electrode (155 mV decade<sup>-1</sup>) was much smaller than those for Ni<sub>2</sub>-O<sub>8</sub>-PcCu/I<sub>2</sub> electrode (194 mV decade<sup>-1</sup>) and Zn<sub>2</sub>-O<sub>8</sub>-PcCu/I<sub>2</sub> electrode (220 mV decade<sup>-1</sup>) (Figure 3e), unambiguously confirming the rapid reaction kinetics of NaI<sub>3</sub> conversion on the Fe<sub>2</sub>-O<sub>8</sub>-PcCu/I<sub>2</sub> electrode.

To gain profound insights into the underlying mechanism on suppressing polyiodide dissolution and accelerating electrochemical redox kinetics, the DFT calculations were performed to investigate the interactions between the PcCu-MOFs and NaI<sub>3</sub> as well as the NaI<sub>3</sub>/I<sub>2</sub> reaction paths on the PcCu-MOFs. First, the charge-density-difference analyses using colored iso-surfaces (Figure 4a) indicated that the conjugated Fe-O<sub>4</sub> centers were the I<sub>3</sub><sup>-</sup> adsorption sites on Fe<sub>2</sub>-O<sub>8</sub>-PcCu because of the relatively stronger polarization interaction at the conjugated Fe-O<sub>4</sub> centers than those at the conjugated -N=C and Cu-N<sub>4</sub> sites.<sup>[50]</sup> The partial density of states (PDOS) calculations demonstrate that the interaction between Fe<sub>2</sub>-O<sub>8</sub>-PcCu and NaI<sub>3</sub>

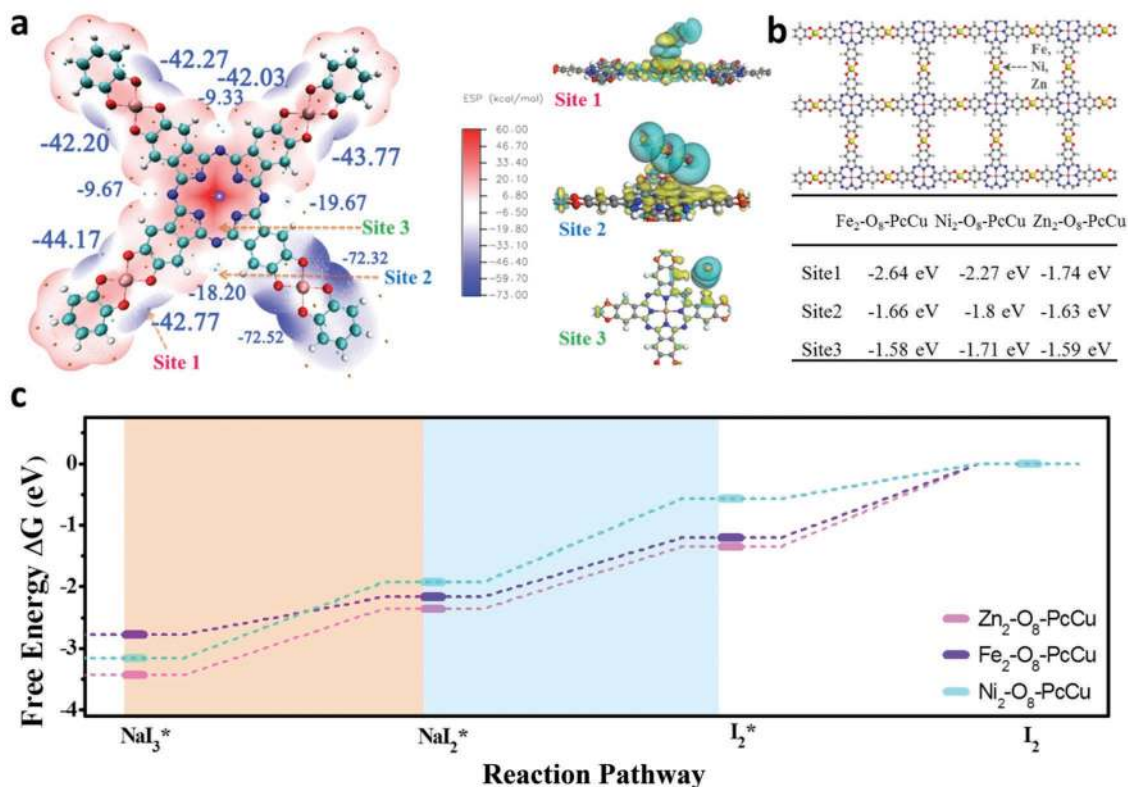


**Figure 4.** First-principles calculations on the underlying mechanism of suppressing polyiodide shuttle dissolution and accelerating electrochemical conversion kinetics. a) The charge-density difference analysis of optimized different sites for polyiodide adsorption in Fe<sub>2</sub>-O<sub>8</sub>-PcCu. b) The comparison of optimized different sites for polyiodide adsorption energy in Fe<sub>2</sub>-O<sub>8</sub>-PcCu, Ni<sub>2</sub>-O<sub>8</sub>-PcCu, and Zn<sub>2</sub>-O<sub>8</sub>-PcCu. c) The calculated free energies of polyiodide oxidation reactions on active centers (conjugated M-O<sub>4</sub> sites, M = Fe, Ni, and Zn) of Fe<sub>2</sub>-O<sub>8</sub>-PcCu, Ni<sub>2</sub>-O<sub>8</sub>-PcCu, and Zn<sub>2</sub>-O<sub>8</sub>-PcCu.

originates from the overlap of the d-orbital of Fe and p-orbital of I<sub>3</sub><sup>-</sup> (Figure S20a, Supporting Information). More specifically, the I<sub>3</sub><sup>-</sup> adsorption energy on Fe-O<sub>4</sub> centers in the Fe<sub>2</sub>-O<sub>8</sub>-PcCu is -2.64 eV, which is lower than those on Ni-O<sub>4</sub> centers (-2.27 eV) in Ni<sub>2</sub>-O<sub>8</sub>-PcCu and Zn-O<sub>4</sub> centers (-1.74 eV) in Zn<sub>2</sub>-O<sub>8</sub>-PcCu (Figure 4b). Furthermore, compared with the Ni-O<sub>4</sub> centers in Ni<sub>2</sub>-O<sub>8</sub>-PcCu and the Zn-O<sub>4</sub> centers in Zn<sub>2</sub>-O<sub>8</sub>-PcCu, the polyiodide adsorption energy on Fe-O<sub>4</sub> centers in the Fe<sub>2</sub>-O<sub>8</sub>-PcCu is much lower than the solvation energy (-2.12 eV) of polyiodide in ethylene carbonate and diethyl carbonate (Figure S20b, Supporting Information). Accordingly, the square planar Fe-O<sub>4</sub> species in Fe<sub>2</sub>-O<sub>8</sub>-PcCu well constrain polyiodide dissolution and thus perform excellent cycle behavior in the Na-I<sub>2</sub> battery. Second, the DFT calculations were performed to evaluate free energies of polyiodide conversion reactions on active centers (M-O<sub>4</sub> sites, M = Fe, Ni, and Zn) of PcCu-MOFs (Figure S21, Supporting Information). The optimized NaI<sub>3</sub>/I<sub>2</sub> reaction path suggested that two endergonic steps involving the NaI<sub>3</sub><sup>\*</sup> oxidation and the I<sub>2</sub><sup>\*</sup> intermediate formation were the rate-limiting steps for whole reaction processes (Figure 4c). The Gibbs free energies for the oxidation of NaI<sub>3</sub><sup>\*</sup> on Fe<sub>2</sub>-O<sub>8</sub>-PcCu was 0.61 eV, which was considerably lower than 1.14 eV for Ni<sub>2</sub>-O<sub>8</sub>-PcCu and 1.15 eV for Zn<sub>2</sub>-O<sub>8</sub>-PcCu, indicating that the polyiodide oxidation conversion was thermodynamically more favorable on the Fe-O<sub>4</sub> centers in Fe<sub>2</sub>-O<sub>8</sub>-PcCu than those on Ni-O<sub>4</sub> centers in Ni<sub>2</sub>-O<sub>8</sub>-PcCu and Zn-O<sub>4</sub> centers in Zn<sub>2</sub>-O<sub>8</sub>-PcCu.<sup>[51]</sup>

Besides the monovalent Na anode, the Fe<sub>2</sub>-O<sub>8</sub>-PcCu/I<sub>2</sub> composites were also coupled with bivalent Zn anodes for Zn-I<sub>2</sub> batteries in the aqueous electrolyte (Figure S22a, Supporting Information). Compared with Na-I<sub>2</sub> batteries, the fabricated Zn-I<sub>2</sub> battery displayed a minor voltage hysteresis of ≈80 mV between anodic and cathodic peaks (Figure S22b, Supporting Information). Even at an extremely high current density of 6.8 A g<sup>-1</sup>, the Zn-I<sub>2</sub> battery using Fe<sub>2</sub>-O<sub>8</sub>-PcCu/I<sub>2</sub> cathode still exhibited a high discharge capacity of 124 mAh g<sup>-1</sup> (Figure S23, Supporting Information). Clearly, the rate capability of Fe<sub>2</sub>-O<sub>8</sub>-PcCu/I<sub>2</sub> cathode for Zn-I<sub>2</sub> battery was superior to that for Na-I<sub>2</sub> battery because the aqueous electrolyte had higher ionic conductivity than the organic electrolyte.<sup>[10,52,53]</sup> Notably, the synthesized conjugated PcCu-MOFs are potential electrode materials for dual-ion batteries because phthalocyanine copper derivatives were recently demonstrated as cathode materials for capacitive-type storage of Li<sup>+</sup> and PF<sub>6</sub><sup>-</sup> with a high specific capacity of 236 mAh g<sup>-1</sup> in a wide voltage range of 1.5–4.5 V versus Li/Li<sup>+</sup>.<sup>[54]</sup> In addition to the above electrochemical energy storage applications, our conjugated PcCu-MOFs are promising materials for electrochemical energy conversion, gas separation/storage, ferromagnetic semiconductors, photocatalysis, etc.<sup>[27,30,55]</sup>

In conclusion, we demonstrated a conjugated Fe<sub>2</sub>-O<sub>8</sub>-PcCu MOF that can suppress the polyiodide dissolution in the Na-I<sub>2</sub> batteries. The operando spectroelectrochemical measurements, electrochemical kinetics analyses, and DFT calculations reveal that the square planar iron-bis(dihydroxy) species in



Fe<sub>2</sub>-O<sub>8</sub>-PcCu act as active centers for simultaneously immobilizing the polyiodide and promoting the reaction kinetics of polyiodide oxidation. Compared with reported cathode materials in Na-I<sub>2</sub> batteries, the Fe<sub>2</sub>-O<sub>8</sub>-PcCu/I<sub>2</sub> electrode exhibits excellent electrochemical performance with a high specific capacity (208 mA g<sup>-1</sup> at 0.3 A g<sup>-1</sup>) and superior long-term cycling stability up to 3200 cycles. Moreover, the PcCu-MOF/I<sub>2</sub> composite can be extended to other metal-I<sub>2</sub> batteries like aqueous multivalent Zn-I<sub>2</sub> batteries with outstanding rate capability. Therefore, this work pays a promising avenue for the design and development of high-performance metal-iodine batteries.

## Supporting Information

Supporting Information is available from the Wiley Online Library or from the author.

## Acknowledgements

F.W., Z.L., and C.Y. contributed equally to this work. The authors thank financial support from the ERC Grant on HIPER-G (Project ID 768930), ERC Starting Grant on FC2DMOF, German Research Foundation (DFG) within the Cluster of Excellence, Center for Advancing Electronics Dresden (cfaed), EU Graphene Flagship (Grant No. CNECT-ICT-604391), and Hamburg Academy of Sciences and Humanities. The authors also thank Dresden Center for Nanoanalysis (DCN) at the Technische Universität Dresden. The authors acknowledge the Center for Information Services and High Performance Computing at Nanjing Tech University and Technische Universität Dresden for computational resources. J.Z. thanks the support of the Fundamental Research Funds for the Central Universities (Grant No. 3102017jc01001). The authors also thank Dr. Gang Wang, Dr. Ali Shaygan Nia, and Dr. Minghao Yu for helpful discussions.

## Conflict of Interest

The authors declare no conflict of interest.

## Keywords

cathode materials, conjugated metal-organic frameworks, Na-I<sub>2</sub> batteries, phthalocyanine copper

Received: August 19, 2019

Revised: October 27, 2019

Published online:

- [1] Z. P. Cano, D. Banham, S. Ye, A. Hintennach, J. Lu, M. Fowler, Z. Chen, *Nat. Energy* **2018**, *3*, 279.
- [2] J. Liu, Y. Zhang, L. Zhang, F. Xie, A. Vasileff, S. Z. Qiao, *Adv. Mater.* **2019**, *31*, 1901261.
- [3] J. L. Ma, F. L. Meng, Y. Yu, D. P. Liu, J. M. Yan, Y. Zhang, X. B. Zhang, Q. Jiang, *Nat. Chem.* **2019**, *11*, 64.
- [4] K. Lu, Z. Hu, J. Ma, H. Ma, L. Dai, J. Zhang, *Nat. Commun.* **2017**, *8*, 527.
- [5] J. Xu, J. Ma, Q. Fan, S. Guo, S. Dou, *Adv. Mater.* **2017**, *29*, 1606454.
- [6] D. Gong, B. Wang, J. Zhu, R. Podila, A. M. Rao, X. Yu, Z. Xu, B. Lu, *Adv. Energy Mater.* **2017**, *7*, 1601885.

- [7] H. Tian, H. Shao, Y. Chen, X. Fang, P. Xiong, B. Sun, P. H. L. Notten, G. Wang, *Nano Energy* **2019**, *57*, 692.
- [8] H. Tian, T. Gao, X. Li, X. Wang, C. Luo, X. Fan, C. Yang, L. Suo, Z. Ma, W. Han, C. Wang, *Nat. Commun.* **2017**, *8*, 14083.
- [9] C. Zhang, Y. Ding, L. Zhang, X. Wang, Y. Zhao, X. Zhang, G. Yu, *Angew. Chem., Int. Ed.* **2017**, *56*, 7454.
- [10] J. Zhang, G. Jiang, P. Xu, A. G. Kashkooli, M. Mousavi, A. Yu, Z. Chen, *Energy Environ. Sci.* **2018**, *11*, 2010.
- [11] C. Xie, Y. Liu, W. Lu, H. Zhang, X. Li, *Energy Environ. Sci.* **2019**, *12*, 1834.
- [12] Q. Zhao, Y. Lu, Z. Zhu, Z. Tao, J. Chen, *Nano Lett.* **2015**, *15*, 5982.
- [13] M. Yu, W. D. McCulloch, D. R. Beauchamp, Z. Huang, X. Ren, Y. Wu, *J. Am. Chem. Soc.* **2015**, *137*, 8332.
- [14] H. Tian, S. Zhang, Z. Meng, W. He, W. Q. Han, *ACS Energy Lett.* **2017**, *2*, 1170.
- [15] Z. Wang, J. Huang, Z. Guo, X. Dong, Y. Liu, Y. Wang, Y. Xia, *Joule* **2019**, *3*, 1289.
- [16] D. F. Sava, M. A. Rodriguez, K. W. Chapman, P. J. Chupas, J. A. Greathouse, P. S. Crozier, T. M. Nenoff, *J. Am. Chem. Soc.* **2011**, *133*, 12398.
- [17] W. Xie, D. Cui, S. R. Zhang, Y. H. Xu, D. L. Jiang, *Mater. Horiz.* **2019**, *6*, 1571.
- [18] Z. Yin, Q. Xin Wang, M. H. Zeng, *J. Am. Chem. Soc.* **2012**, *134*, 4857.
- [19] M. G. Campbell, S. F. Liu, T. M. Swager, M. Dincă, *J. Am. Chem. Soc.* **2015**, *137*, 13780.
- [20] D. Sheberla, J. C. Bachman, J. S. Elias, C. J. Sun, Y. Shao-Horn, M. Dincă, *Nat. Mater.* **2017**, *16*, 220.
- [21] D. Feng, T. Lei, M. R. Lukatskaya, J. Park, Z. Huang, M. Lee, L. Shaw, S. Chen, A. A. Yakovenko, A. Kulkarni, J. Xiao, K. Fredrickson, J. B. Tok, X. Zou, Y. Cui, Z. Bao, *Nat. Energy* **2018**, *3*, 30.
- [22] J. Chen, K. Zou, P. Ding, J. Deng, C. Zha, Y. Hu, X. Zhao, J. Wu, J. Fan, Y. Li, *Adv. Mater.* **2019**, *31*, 1970014.
- [23] H. Wang, Q. L. Zhu, R. Zou, Q. Xu, *Chem* **2017**, *2*, 52.
- [24] L. Sun, M. G. Campbell, M. Dincă, *Angew. Chem., Int. Ed.* **2016**, *55*, 3566.
- [25] J. Ran, J. Qu, H. Zhang, T. Wen, H. Wang, S. Chen, L. Song, X. Zhang, L. Jing, R. Zheng, S. Z. Qiao, *Adv. Energy Mater.* **2019**, *9*, 1803402.
- [26] L. Zou, C. C. Hou, Z. Liu, H. Pang, Q. Xu, *J. Am. Chem. Soc.* **2018**, *140*, 15393.
- [27] C. Yang, R. Dong, M. Wang, P. S. Petkov, Z. Zhang, M. Wang, P. Han, M. Ballabio, S. A. Bräuninger, Z. Liao, J. Zhang, F. Schwotzer, E. Zschech, H. H. Klauss, E. Cánovas, S. Kaskel, M. Bonn, S. Zhou, T. Heine, X. Feng, *Nat. Commun.* **2019**, *10*, 3260.
- [28] R. Dong, P. Han, H. Arora, M. Ballabio, M. Karakus, Z. Zhang, C. Shekhar, P. Adler, P. St. Petkov, A. Erbe, S. C. B. Mannsfeld, C. Felser, T. Heine, M. Bonn, X. Feng, E. Cánovas, *Nat. Mater.* **2018**, *17*, 1027.
- [29] N. Han, Y. Wang, L. Ma, J. Wen, J. Li, H. Zheng, K. Nie, X. Wang, F. Zhao, Y. Li, J. Fan, J. Zhong, T. Wu, D. J. Miller, J. Lu, S. T. Lee, Y. Li, *Chem* **2017**, *3*, 652.
- [30] H. Zhong, K. H. Ly, M. Wang, Y. Krupskaya, X. Han, J. Zhang, J. Zhang, V. Kataev, B. Büchner, I. M. Weidinger, S. Kaskel, P. Liu, M. Chen, R. Dong, X. Feng, *Angew. Chem., Int. Ed.* **2019**, *58*, 10677.
- [31] S. S. Shinde, C. H. Lee, J. Y. Jung, N. K. Wagh, S. H. Kim, D. H. Kim, C. Lin, S. U. Lee, J. H. Lee, *Energy Environ. Sci.* **2019**, *12*, 727.
- [32] M. Kumar, V. Bhatt, O. S. Nayal, S. Sharma, V. Kumar, M. S. Thakur, N. Kumar, R. Bal, B. Singh, U. Sharma, *Catal. Sci. Technol.* **2017**, *7*, 2857.
- [33] C. Xia, J. Guo, P. Li, X. Zhang, H. N. Alshareef, *Angew. Chem., Int. Ed.* **2018**, *57*, 3943.
- [34] Y. Fang, X. Y. Yu, X. W. Lou, *Adv. Mater.* **2018**, *30*, 1706668.
- [35] F. Yu, T. Huang, P. Zhang, Y. Tao, F. Z. Cui, Q. Xie, S. Yao, F. Wang, *Energy Storage Mater.* **2019**, *22*, 235.

- [36] Y. Zhao, L. Wang, H. R. Byon, *Nat. Commun.* **2013**, *4*, 1896.
- [37] S. Kim, S. K. Kim, P. Sun, N. Oh, P. V. Braun, *Nano Lett.* **2017**, *17*, 6893.
- [38] G. Nikiforidis, K. Tajima, H. R. Byon, *ACS Energy Lett.* **2016**, *1*, 806.
- [39] Z. Su, Z. Wei, C. Lai, H. Deng, Z. Liu, J. Ma, *Energy Storage Mater.* **2018**, *14*, 129.
- [40] X. Tang, D. Zhou, P. Li, X. Guo, C. Wang, F. Kang, B. Li, G. Wang, *ACS Cent. Sci.* **2019**, *5*, 365.
- [41] K. Li, Z. Hu, J. Ma, S. Chen, D. Mu, J. Zhang, *Adv. Mater.* **2019**, *31*, 1902399.
- [42] F. Bertasi, F. Sepehr, G. Pagot, S. J. Paddison, V. D. Noto, *Adv. Funct. Mater.* **2016**, *26*, 4860.
- [43] Y. Li, L. Liu, H. Li, F. Cheng, J. Chen, *Chem. Commun.* **2018**, *54*, 6792.
- [44] H. Pan, B. Li, D. Mei, Z. Nie, Y. Shao, G. Li, X. S. Li, K. S. Han, K. T. Mueller, V. Sprenkle, J. Liu, *ACS Energy Lett.* **2017**, *2*, 2674.
- [45] B. Li, Z. Nie, M. Vijayakumar, G. Li, J. Liu, V. Sprenkle, W. Wang, *Nat. Commun.* **2015**, *6*, 6303.
- [46] C. Xie, H. Zhang, W. Xu, W. Wang, X. Li, *Angew. Chem., Int. Ed.* **2018**, *57*, 11171.
- [47] J. M. Gardner, M. Abrahamsson, B. H. Farnum, G. J. Meyer, *J. Am. Chem. Soc.* **2009**, *131*, 16206.
- [48] S. K. Jung, H. Kim, M. G. Cho, S. P. Cho, B. Lee, H. Kim, Y. U. Park, J. Hong, K. Y. Park, G. Yoo n, W. M. Seong, Y. Cho, M. H. Oh, H. Kim, H. Gwon, I. Hwang, T. Hyeon, W. S. Yoon, K. Kang, *Nat. Energy* **2017**, *2*, 16208.
- [49] F. Faisal, C. Stumm, M. Bertram, F. Waidhas, Y. Lykhach, S. Cherevko, F. Xiang, M. Ammon, M. Vorokhta, B. Šmíd, T. Skála, N. Tsud, A. Neitzel, K. Beranová, K. C. Prince, S. Geiger, O. Kasian, T. Wähler, R. Schuster, M. A. Schneider, V. Matolín, K. J. J. Mayrhofer, O. Brummel, J. Libuda, *Nat. Mater.* **2018**, *17*, 592.
- [50] B. W. Zhang, T. Sheng, Y. X. Wang, S. Chou, K. Davey, S. X. Dou, S. Z. Qiao, *Angew. Chem., Int. Ed.* **2019**, *58*, 1484.
- [51] Z. Du, X. Chen, W. Hu, C. Chuang, S. Xie, A. Hu, W. Yan, X. Kong, X. Wu, H. Ji, L. J. Wan, *J. Am. Chem. Soc.* **2019**, *141*, 3977.
- [52] Y. Tao, C. Ding, D. Tan, F. Yu, F. Wang, *ChemSusChem* **2018**, *11*, 4269.
- [53] F. Wang, H. Yang, J. Zhang, P. Zhang, G. Wang, X. Zhuang, G. Cuniberti, X. Feng, *Adv. Mater.* **2018**, *30*, 1800028.
- [54] H. Wang, H. Wang, Z. Si, Q. Li, Q. Wu, Q. Shao, L. Wu, Y. Liu, Y. Wang, S. Song, H. Zhang, *Angew. Chem., Int. Ed.* **2019**, *58*, 10204.
- [55] R. Chen, J. L. Shi, Y. Ma, G. Lin, X. Lang, C. Wang, *Angew. Chem., Int. Ed.* **2019**, *58*, 6430.